11th International Symposium on Turbulence and Shear Flow Phenomena (TSFP11)
Southampton, UK, July 30 to August 2, 2019

FORMATION AND TRANSITION OF ORIFICE–GENERATED VORTEX RINGS

R. Limbourg and J. Nedić*
Department of Mechanical Engineering
McGill University, 817 Sherbrooke St W
Montreal, QC H3A 0C3, Canada
*jovan.nedic@mcgill.ca

ABSTRACT

The influence of initial conditions on the formation mechanisms and transition of orifice–generated vortex rings is investigated using flow visualisations and time-resolved planar Particle Image Velocimetry. Stroke ratios between $0.4 \le L_0/D_0 \le 9$ and Reynolds numbers ranging between $10^3 \le Re_{L_0} = U_0 L_0/(2\nu) \le 10^5$ were investigated. Compared to nozzle–generated vortex rings, the laminar-turbulent transition line for orifice–generated vortex rings was found to be at lower Reynolds numbers, with no laminar vortex rings being created for the range considered. The total circulation of the flow field and the circulation of the vortex ring were investigated to determine the formation time of orifice–generated vortex rings. The formation numbers was found to be $1.0-1.5$, which are noticeably different from those determined by Gharib *et al.* (1998) for nozzle–generated vortex rings. It was observed that the circulation of the isolated vortex ring, once it has pinched–off from the shear layer, had a constant asymptotic value when normalized using the diameter of the orifice and the translational speed of the vortex ring U_0. The total circulation in the flow-field was found to scale with the slug–length L_0.

INTRODUCTION

Vortex rings are ubiquitous in nature, ranging from animal locomotion to cardiac flows, and are considered an archetypal flow in which instabilities develop and breakdown during transition. Experimentally, vortex rings are generated by a brief discharge of fluid through a sharp-edged nozzle or an orifice, as shown in Figure 1. As the column of fluid is impulsively discharged into the quiescent surroundings by the impulsive motion of a piston, the shear imposed by the turning angle, α, forces a sheet of vorticity to curl and roll up into a vortex ring. A significant body of work has focussed on understanding the formation process of laminar vortex rings from nozzle geometries, as well as its transition into a turbulent state.

An oft–used model for the discharged fluid emanating from the nozzle exhaust is the slug-flow model, which assumes that the fluid is discharged as a column with a diameter of D_p and a length of L_p, where D_p is the diameter of the piston and $L_p = U_p t$ is the stroke length of the piston, *i.e.*, the distance travelled by the piston moving at a speed of U_p over a time-frame of t. One of the main assumptions in this model is that the velocity profile at the exhaust is top-hat and that the velocity vectors are parallel to each other and the main translational axis. The predicted circulation from the slug-flow model is given as $\Gamma = \frac{1}{2} U_p L_p$. Measurements of the velocity profile at the exhaust of the nozzle were investigated by Didden (1979), who demonstrated the clear influence of boundary conditions, namely boundary layer effects, on the shape of the profile which in turn produced circulation values that were inconsistent with the slug-flow model. The direct numerical simulation study of James & Madnia (1996) and the numerical vortex-sheet model approach of Nitsche & Krasny (1994) confirmed Didden (1979) findings. Cater *et al.* (2004) complemented the work of Didden (1979) by showing the influence of the piston vortex on the vortex rings formation.

As fluid is continuously ejected from the orifice, a critical dimensionless time is observed where the vortex ring eventually detaches, or "pinches–off", from the feeding shear layer, resulting in an isolated vortex ring. The formation time, or number, of this process has been the focus of several studies. Using the Kelvin-Benjamin variational principle (Benjamin, 1976), Gharib *et al.* (1998) proposed an energy-based interpretation for the pinch–off mechanism in which there was a maximum amount of energy a vortex ring can attain and that there was a universal timescale associated with this process. The formation time, defined as $t/(D_p/U_p)$ or equivalently $L_p(t)/D_p$ where $L_p(t)$ is the instantaneous length of the column of fluid discharged from the exhaust, was found to be between $3.6 \le L_p/D_p \le 4.5$ for nozzle geometries. For values greater than $L_p/D_p \approx 4.5$, vorticity would be left behind in the flow field in the form of a trailing jet. Numerous studies have confirmed this finding (*e.g.* Krueger & Gharib (2003), Aydemir *et al.* (2012)) and have even found to hold for synthetic jets from noz-

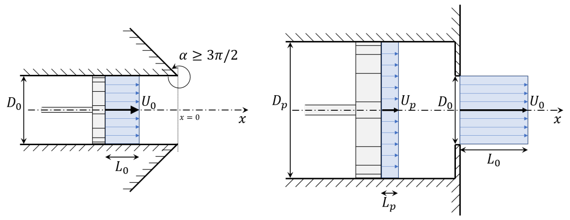

Figure 1. Nozzle geometry (left) and orifice geometry (right) apparatus with simplified slug-model flow at the exhaust. The schematic is made to scale for a discharged duration of 1 s.

zles (Lawson & Dawson, 2013) and vortex rings detaching from disks (Fernando & Rival, 2016). Rosenfeld *et al.* (1998) complemented the findings of Gharib *et al.* (1998) by numerically investigating the influence of the velocity program, velocity profile and Reynolds number on the formation process of laminar rings generated by three types of nozzle geometries. They found that the formation number can be modified by the initial conditions; for example, a constant acceleration velocity program yields to a formation number of 5.22, whereas a parabolic velocity profile reduces the formation number to 0.90. This value is lower than the 1.42 reported by Zhao *et al.* (2000), but it nevertheless highlights the clear effects the inlet velocity profile has on the formation time.

Compared to the numerous studies investigating the formation of nozzle–generated vortex rings, there is limited knowledge on the formation number of orifice–generated vortex rings. Gan & Nickels (2010), for example, investigated orifice–generated turbulent vortex rings with a $L_0/D_0 = 3.43$ and observed a trailing jet behind the primary vortex. Note that the values D_0 and L_0 correspond to the diameter and slug-length from the exhaust and are not equal to the piston diameter and piston stroke length in this configuration (see Figure 1). The observation of a trailing jet for L_0/D_0 values below those found in the literature was attributed to either the formation of stronger initial vortices due to the higher initial speed, or to the boundary conditions imposed by the orifice geometry. The expected difference in the outlet velocity profile created by an orifice and nozzle geometry, for identical volume flow rates, was noted by Saffman (1978) and Pullin (1979) who developed a model for the maximum circulation. A correction to the slug-flow model to account for "over-pressure" effects at low L_0/D_0 was developed by Krueger (2005) and later validated numerically by Krueger (2008). Krieg & Mohseni (2013) further modified the slug-model to account for the effects of non-parallel outlet velocity profiles, such as those found in orifice geometries.

Given the clear effects an orifice geometry has on the outlet velocity profile, one might expect a formation number different to those observed in nozzle geometries. To the best of our knowledge, the formation number of orifice–generated vortex rings has not been reported in the literature; one of the main objectives of this work is to therefore determine this formation number. A second objective of this work is concerned with the more practical aspect of knowing the conditions under which a vortex ring formed from an orifice geometry would be laminar, transitional or turbulent; in essence, we wish to create a transition map similar to the one created by Glezer (1988) for nozzle–generated vortex rings.

EXPERIMENTAL SETUP

Experiments were conducted in a 2.0 m-long water tank with a 80 cm × 90 cm cross-sectional area. A 12.7 cm diameter hole is cut into one end of the tank into which an acrylic tube with a 10.2 cm inner diameter is mounted. Water is pushed by an electric linear actuator (modified version of ServoCylinder A2, Ultra Motion). The piston has a maximum stroke length of 32.4 cm and a maximum speed of 60 cm/s. The piston head is sealed with rubber O-rings; a silicon-based lubricant is used to reduce the friction and eliminate jolts during the initial acceleration. A 15.2 cm-diameter flange is attached to the tube and the exhaust is covered with a 2.4 mm-thick aluminium sheet into which various orifice shapes are laser cut. Two high-speed cameras (Photron FASTCAM Mini WX50) are used to visualise and record the formation process and the propagation of the vortex ring. One camera is set to record the formation at the edge of the orifice and the second one is placed at $10D_0$ from the exhaust.

For a given orifice plate, the diameter D_0 of the orifice and the tube diameter D_p are fixed (Figure 1). Because the input to the experiments are the piston speed U_p and the piston stroke length L_p, the speed of the discharged fluid at the exhaust of the orifice U_0 and the 'slug length' L_0 (see Figure 1) are computed using the conservation of mass (or volume since density is assumed constant):

$$D_p^2 U_p = D_o^2 U_o \Leftrightarrow L_p D_p^2 = L_0 D_0^2$$

In order to determine the transition map, blue food colouring was used to visualise the vortex. Although dye can be a misleading flow marker in the case of slow flows (Maxworthy, 1972), it is less of a concern in our study considering the relative high convective speeds. Measurements were taken for circulation-based Reynolds numbers $Re_{L_0} = U_0 L_0/(2\nu) = \Gamma_0/\nu$, where $\Gamma_0 = U_0 L_0/2$ is the initial fluid circulation and ν is the kinematic viscosity of water, between $10^3 \leq Re_{L_0} \leq 10^5$. The stroke–ratio L_0/D_0 was also varied between $1 \leq L_0/D_0 \leq 10$. Note that we define our circulation-based Reynolds number based on the properties of the discharged fluid from the orifice, as opposed to the piston, in order to maintain dynamic similarity with previous measurements using nozzle geometries.

To study the formation process, the velocity field was obtained using time-resolved planar Particle Image Velocimetry (TR-2D2C PIV). A field of view of $3.8D_0 \times 3.8D_0$, focused on the exhaust of the orifice plane containing the axis of symmetry of the ring, was employed and illuminated with a high-speed ND:YLF laser (Litron Laser LDY302 PIV series). The high-speed camera was set at a sample rate of 250 Hz, for an equivalent temporal resolution of $\Delta t = 4.0$ ms. The TR-2D2C PIV cross-correlation processing is managed with DaVis 10 (LaVision GmbH) software. Image preprocessing was applied to filter out the noise from the PIV images. A four-pass cross-correlation scheme was then applied ending in a 24×24 px interrogation area with a 75% overlap. This results in a 341×341 vector field equally spaced with $\Delta x = 0.58$ mm $\approx 0.011D_0$. Four sets of experiments were carried out corresponding to increasing values of the L_0/D_0 ratio; 1.0 for an isolated ring *i.e.* no trailing jet is observed, 2.0, 2.5 and 3.0 where the ring is clearly followed by a trailing jet. For each L_0/D_0 ratio, the dependence to the circulation-based Reynolds number $Re_{L_0} = U_0 L_0/(2\nu) = \Gamma_0/\nu$ was tested.

RESULTS AND DISCUSSION

Transition map

For nozzle geometries, Glezer (1988) investigated fully turbulent vortex rings with the aim of highlighting the parameters that influence the onset of turbulence and created a transition map based on initial parameters such as the nozzle diameter D_p (= 1.00 in or 0.75 in), the piston stroke length L_p and the speed of the discharged fluid U_p. The state of the vortex ring was characterised by its circulation-based Reynolds number Re_{L_0} and the stroke-ratio L_0/D_0; for nozzle–generated vortex rings $Re_{L_p} \equiv Re_{L_0}$. The main transition line of Glezer (1988), taken at a downstream loca-

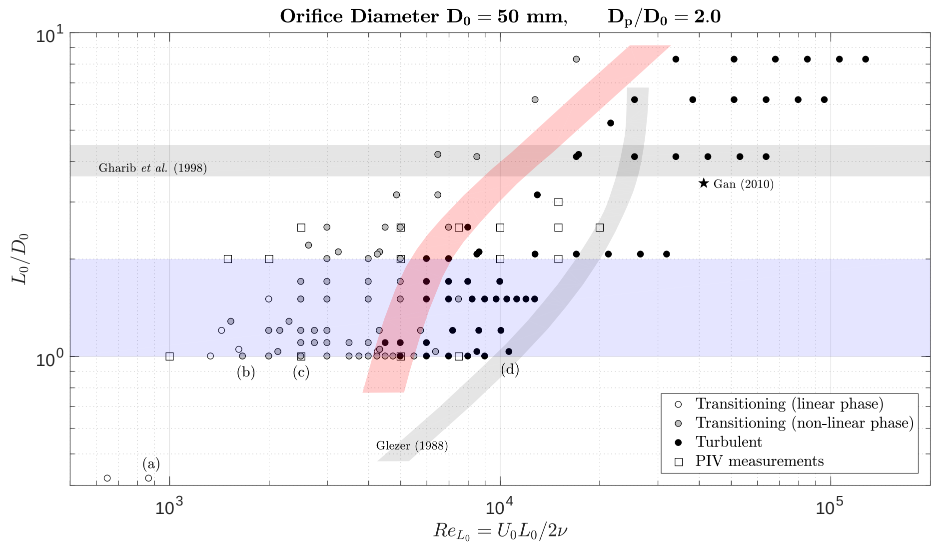

Figure 2. Transition map at $x = 10D_0$ for a orifice plate with outlet diameter $D_0 = 50$ mm. Oblique grey shaded line shows transition line for nozzle geometry, taken from Glezer (1988). Horizontal grey shaded band corresponds to Gharib *et al.* (1998)'s formation number limiting value. Red shaded line corresponds to the approximate transition line for the current measurements. Blue shaded line corresponds to the approximate formation number limiting value for current measurements. Letters (a), (b), (c) and (d) correspond to Figure 3.

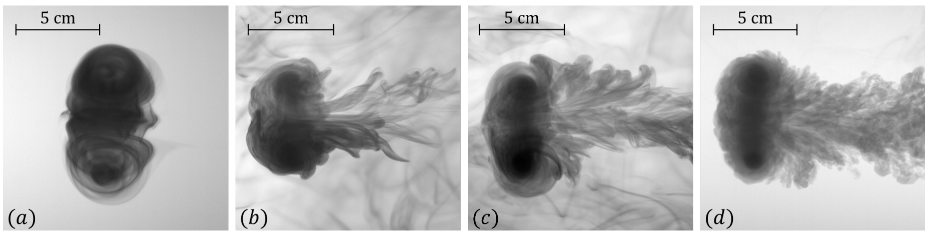

Figure 3. Transitioning vortex rings in the (a) linear phase ($L_0/D_0 = 0.42$ and $U_0 = 83$ mm/s and $Re_{L_0} = 875$), (b) in the early non-linear phase ($L_0/D_0 = 1.0$ and $U_0 = 67$ mm/s and $Re_{L_0} = 1,675$), (c) in the late non-linear phase ($L_0/D_0 = 1.0$ and $U_0 = 100$ mm/s and $Re_{L_0} = 2,500$) and (d) Turbulent vortex ring ($L_0/D_0 = 1.0$ and $U_0 = 413$ mm/s and $Re_{L_0} = 10,325$).

tion of $x = 20D_0$, is shown in Figure 2 as an oblique shaded curve. The state of an orifice–generated vortex ring at a downstream location of $x = 10D_0$, for a orifice diameter of $D_0 = 50$ mm, are also shown in this figure, along with the formation number of Gharib *et al.* (1998).

For the experimental range considered here, no laminar ring was observed by $x = 10D_0$. It is believed that the orifice plate introduces a large turning radius for the fluid which in turn triggers instabilities at the orifice *e.g.* Kelvin-Helmholtz instabilities, which would force the laminar vortex ring to transition. The characterisation of transitioning rings is somewhat complicated since it involves two processes. First, during the linear phase, azimuthal waves develop around the core ring and the toroidal structure is twisted into a 'star-like' ring, easily identified in a cross-sectional plane (see Figure 3(a)). During the second non-linear phase, secondary structures develop around the core and are shed intermittently into the wake as hairpin vortices (Figure 3(b) & 3(c)). Turbulent vortex rings are visually characterised by a chaotic vortex core and trailing wake, as shown in Figure 3(d). Differentiating between a late transitioning ring and a fully turbulent ring is relatively subjective. Whereas the wake of a fully turbulent ring is chaotic, orderly filaments of dye are still visible in the wake of a transitioning ring. This is the criterion presently used to discriminate fully turbulent rings from transitioning rings in the non-linear phase.

Glezer's transition line between laminar and turbulent vortex rings indicates a $+1$-slope for low values of L_0/D_0, suggesting that the dominant parameter in this region of the map is $Re_{D_0} = U_0 D_0 / 2\nu$. For large L_0/D_0, the transition line reaches a vertical asymptote with a corresponding $Re_{L_0} \approx 25,000$. In the present study, the results indicate the inverse to be true, with a vertical asymptote for low L_0/D_0 and an oblique asymptote of slope $+1$ for high L_0/D_0 can be observed. It is also evident from Figure 2 that the transition line has been noticeably shifted toward lower values Re_{L_0}. It is important to remember that the transition line shown for the current measurements correspond to vortex rings which are considered fully turbulent and those that are in the non-linear phase of transition. It is therefore evident that the transition line from laminar to turbulent vortex rings is considerably lower than what was predicted by Glezer for a nozzle geometry. As stated earlier, it is believed that the orifice geometry itself causes Kelvin-Helmholtz instabilities to form during the formation process and hence force the vortex ring to transition earlier, compared to nozzle geometries. Evidence of this can be seen, for example, in Figure 4(d), where the shear layer from the exhaust has clearly broken down into numerous vortex rings. In essence, the initial conditions are expected to affect the state of a vortex ring at a particular downstream location, which was also

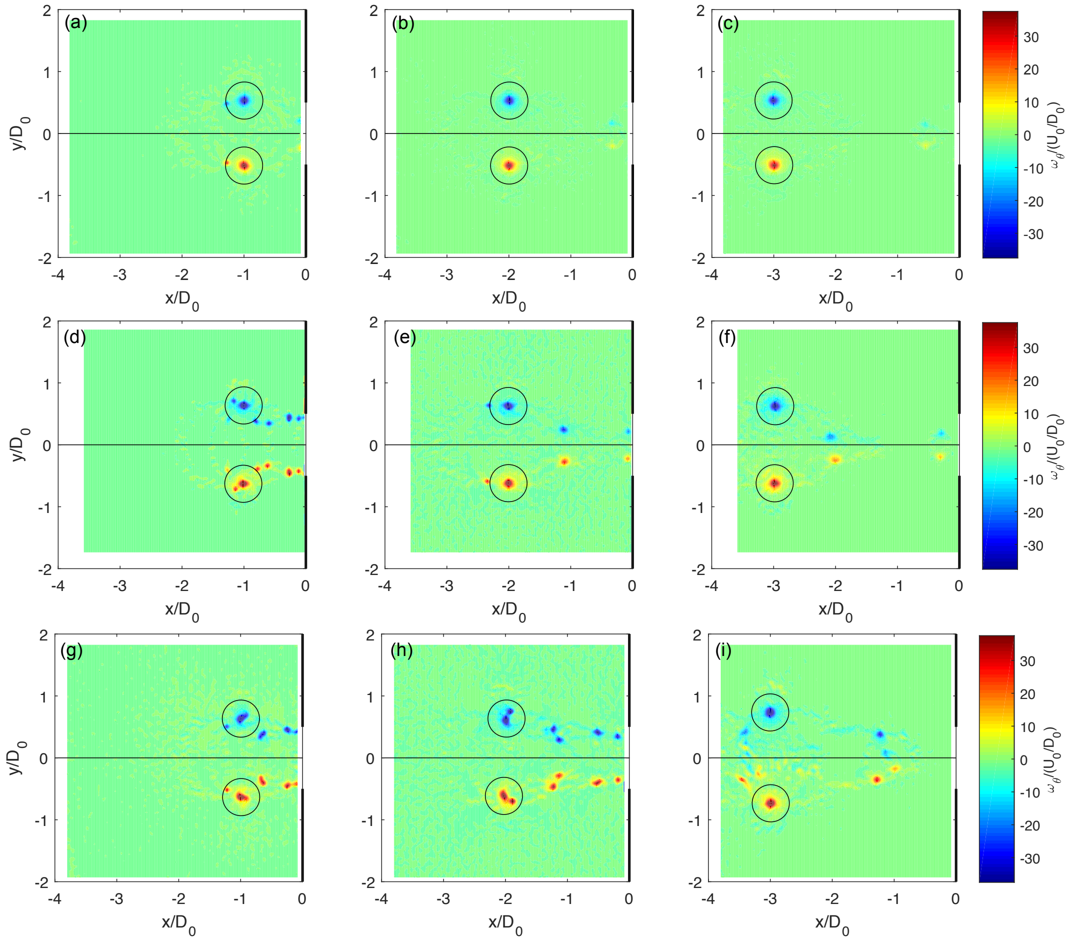

Figure 4. Normalised azimuthal vorticity $\omega_\theta/(U_0/D_0)$ at three downstream locations $x/D_0 = -1$, $x/D_0 = -2$ and $x/D_0 = -3$ from the orifice, for stroke-ratios of $L_0/D_0 = 1$ (a-c), $L_0/D_0 = 2$ (d-f) and $L_0/D_0 = 3$ (g-i). Vortex ring is moving from right to left.

stated by Glezer. One final aspect that is worth noting for the transition map is that its findings are clearly dependant upon the location where the vortex ring is observed; a vortex ring that is laminar at $x = 5D_0$ might be in a transitional state by $x = 10D_0$ and turbulent by $x = 20D_0$. Nevertheless, given that no laminar vortex rings were observed at all Reynolds numbers considered here, and that fully turbulent vortex rings were observed for lower Reynolds numbers at a closer downstream distance from the orifice ($x = 10D_0$ here compared to $x = 20D$ for Glezer), we conclude that the transition line for orifice–generated vortex rings occurs at lower Reynolds numbers compared to nozzle–generated vortex rings.

Circulation and formation time

The formation time of a vortex ring, as defined by Gharib *et al.* (1998), is based on the time it takes for a vortex ring to attain its maximum possible energy. Equivalently, one could use the vorticity of the flow-field, and hence the circulation, to investigate the formation process of a vortex ring. By comparing the circulation of an isolated vortex ring, which would reach a constant asymptotic value, to that of the total circulation in the flow-field, one can find the formation time by tracing the circulation of the isolated vortex ring back in time to see where it intersects the total circulation curve.

Figure 4 shows the vorticity contours for three stroke-ratios, $L_0/D_0 = 1$, 2 and 3, at three downstream locations. The boundaries of the field of view are sufficiently far from the core ring to consider the total circulation of the flow to be contained within the field of view. Assuming symmetry, the total circulation can be computed from either half of the domain. In our study, the total circulation is computed by integrating the azimuthal vorticity within each half plane and taking the average of the absolute value of the two halves.

The total circulation, normalised by the slug-length circulation $U_0L_0/2$ (Glezer, 1988), of the three stroke-ratios as a function of non-dimensional time t^* (which is equivalent to $L_0(t)/D_0$) is shown in Figure 5. Note that the Reynolds number based on the slug-length L_0 increases from 5,000 to 15,000, whilst the Reynolds number based on orifice diameter D_0 is fixed. For all three cases, the circulation increases linearly before reaching a constant value; the transition from one region to another is demarcated by the stroke-ratio of the piston. Two observations can been made for the total circulation; the first is that the total circulation is almost 2.5 times greater that predicted by the slug-model, the second is that the normalised total circulations appears, at least at first glance, to asymptote to similar values. The disparity with slug-model predications can be explained by the initial velocity profile not exhibiting a top-hat profile, which was verified by examining the PIV data close to the exhaust. It is worth noting that for nozzle geometries, the slug model underestimates the circulation for

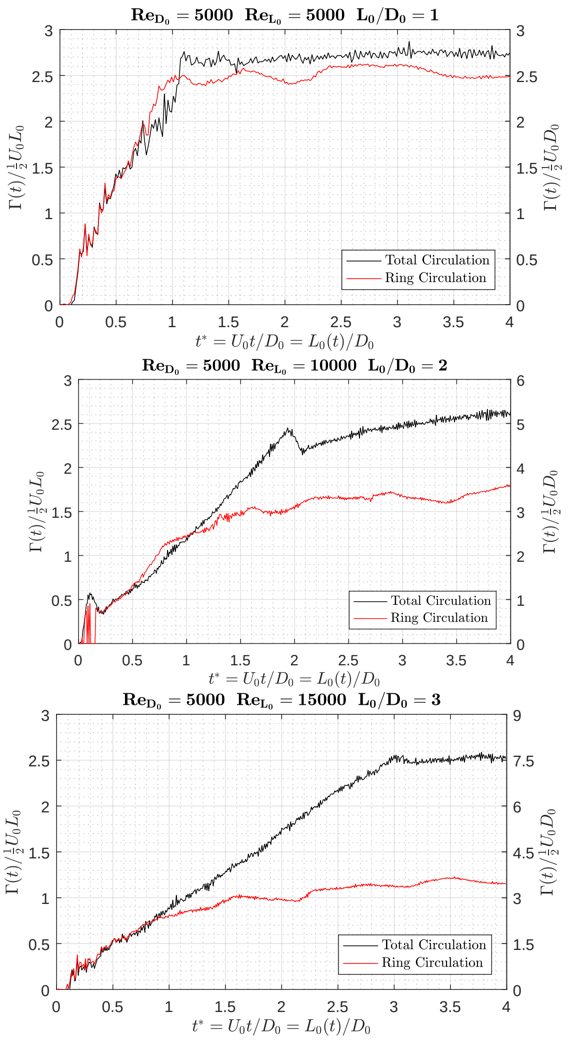

Figure 5. Variation of normalized circulation $2\Gamma(t)/(U_0L_0)$ (or equivalently $2\Gamma(t)/(U_0D_0)$) as a function of the formation time t^* for a fixed diameter-based Reynolds number $Re_{D_0} = U_0D_0/(2\nu) = 5{,}000$. Total circulation shown in black and ring circulation shown in red.

low Reynolds numbers ($Re_{L_0} < 7{,}000$) and overestimates for higher Reynolds number ($Re_{L_0} > 30{,}000$) (Shariff & Leonard, 1992). The asymptotic values of the total circulation appear to settle to roughly similar values, ranging between 2.7 for $L_0/D_0 = 1$ to 2.5 for $L_0/D_0 = 3$. Further measurements would need to be taken to ascertain if the scaling law for the normalised total circulation, developed by Saffman (1978) and Pullin (1979), do indeed hold.

A key challenge in determining the ring circulation is selecting the appropriate boundaries over which the circulation is calculated. In this study, the ring circulation is calculated around a circular boundary centred on the core of the vortex, as shown in Figure 4. At each time-step, the location of the vortex core centre is found and a two-dimensional Gaussian function is fitted to the vorticity data. The width of the Gaussian fit is calculated and the boundary is set to be five times this value. The ring circulation as a function of time is shown in Figure 5. For the $L_0/D_0 = 1$ case, it is clear that the total circulation and ring circulation are equal; this is corroborated with the date from Figure 4 (a-c), where no excess vorticity is observed outside

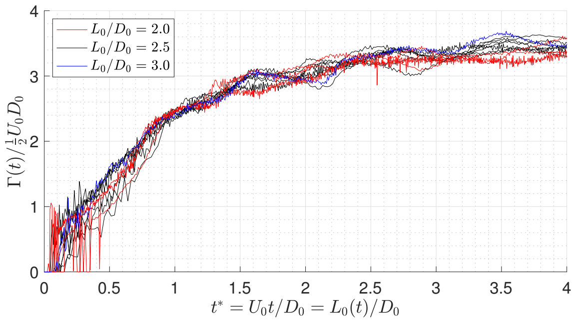

Figure 6. Normalized ring circulation $2\Gamma(t)/(U_0D_0)$ as a function of the formation time t^* for diameter-based Reynolds number between $2{,}000 \leq Re_{D_0} \leq 8{,}000$ and stroke-ratios of $L_0/D_0 = 2,\ 2.5,\ 3$.

the primary vortex ring. This would indicate that the vortex ring has not achieved its maximum energy level. As the stroke length is increased to $L_0/D_0 = 2$, a clear distinction is noted between the total circulation and the ring circulation, with the ring circulation settling to a normalized circulation of $\tilde{\Gamma}_{L_0} = 2\Gamma(t)/U_0L_0 \approx 1.6$. The excess vorticity, which is clearly separate from the primary vortex ring, can be seen in Figure 4 (d-f). Increasing the stroke-ratio further to $L_0/D_0 = 3$ we again see a clear difference between the total circulation and the ring circulation in Figure 5, as well as the excess vorticity in Figure 4 (g-i). It is therefore evident that the vortex ring has attained its maximum energy and has pinched-off from the attaching shear layer. The ring circulation for the $L_0/D_0 = 3$ case is found to be $\tilde{\Gamma}_{L_0} \approx 1.1$. Note that the stepwise change in ring circulation is due to secondary vortex rings catching up with the primary ring, which are sometimes entrained in the primary ring. It was verified for the cases shown here that by $x/D_0 = 3$, the convective speed and acceleration of the trailing vortices was sufficiently low that we would not expect it to catch up to the primary vortex ring further downstream.

One major concern with normalising the ring circulation with the slug-model circulation is that the slug-model circulation does not take into account the dynamics of an isolated vortex ring that has achieved its maximum energy. A more appropriate normalisation would be one that includes a length-scale associate with the vortex ring itself; the diameter of the orifice is a suitable choice given that one would expect the vortex ring diameter to be proportional to the orifice diameter (as opposed to the slug length). The normalised circulation using the orifice diameter, $\tilde{\Gamma}_{D_0} = 2\Gamma(t)/U_0D_0$, is shown on the second y-axis in Figure 5. Using this scaling we observe that the asymptotic value for the total circulation increases with increasing stroke-ratio, whilst the ring circulation (for a fully formed vortex ring) are similar for the $L_0/D_0 = 2$ and 3 cases, with values of $\tilde{\Gamma}_{D_0} \approx 3.2 - 3.3$. This finding further strengthens our belief, and that of Rosenfeld *et al.* (1998), that the dynamics of the vortex ring should be scaled using the diameter of the orifice.

The results in Figure 5 are for a fixed Re_{D_0} and hence to determine if there is any Reynolds number dependance on the asymptotic normalized ring circulation value, measurements were taken between $2{,}000 \leq Re_{D_0} \leq 8{,}000$ for $L_0/D_0 = 2.0$ ($4{,}000 \leq Re_{L_0} \leq 16{,}000$), $L_0/D_0 = 2.5$ ($5{,}000 \leq Re_{L_0} \leq 20{,}000$) and $L_0/D_0 = 3.0$ ($6{,}000 \leq Re_{L_0} \leq 24{,}000$). The normalised ring circulations $\tilde{\Gamma}_{D_0}$ are shown in Figure 6, where we note that all the data points collapse onto similar curves whose asymptote is roughly 3.2-3.6.

Finally, we investigate the formation number of orifice–generated vortex rings by tracing back the ring circulation value to point where it intersects the total circulation curve, as done by Gharib *et al.* (1998). For all cases considered here, the formation number was found to lie between 1.3 - 1.5. This is considerably lower than those found in the literature for nozzle–generated vortex rings, which are between 3.6 - 4.5. Although low formation numbers of around 1 have been observed for vortex rings whose initial velocity profile was parabolic (Rosenfeld *et al.*, 1998), this was not evident for the current measurements, although the did exhibit a strong curvature similar to what has been observed in the orifice–generated vortex ring literature (Krueger, 2005, 2008; Krieg & Mohseni, 2013). The exact reason for why the formation number is lower is still unknown, however, we postulate that the break-up of the shear layer from the exhaust due to Kelvin-Helmholtz instabilities, as well as the velocity profile, play a key role.

CONCLUSION

The formation and transition of orifice–generated vortex rings was experimentally investigated using a combination of flow visualisation experiments and time-resolved particle image velocimetry in the Reynolds number range of $10^3 \leq Re_{L_0} \leq 10^5$ and stroke–ratios of $0.4 \leq L_0/D_0 \leq 9$. Vortex rings generated by a nozzle geometry have been extensively studied and well documented in the literature, however, our knowledge of orifice–generated vortex rings is significantly less extensive. A major difference between the two geometries is the step-change in diameter of the piston, used to impulsively push the fluid out of the exhaust, and the diameter of the exhaust. This step-change in diameter forces the fluid to undergo a significant turning radius both upstream and downstream of the exhaust; as such, the velocity profile no longer exhibits a top–hat–like velocity profile at the exhaust, which is a characteristic of nozzle–generated vortex rings and a key component of the slug-flow model for vortex rings. Moreover, Kelvin-Helmholtz instabilities are created which in turn trigger transition at a lower Reynolds numbers compared to those observed in nozzle geometries; no purely laminar rings were observed for the conditions considered, with vortex rings either exhibiting a transitional state or were fully turbulent by $x = 10D_0$.

The formation number was found by measuring the circulation of the isolated vortex ring and tracing it back in time to corresponding circulation of the the entire flow field. It was found that the formation number lies in the range of 1.0 - 1.5, which is significantly lower than the values of 3.6 - 4.5 observed by Gharib *et al.* (1998). It is believed that this lower formation number is due to the large curvature in the initial velocity profile and the break up of the shear layer due to Kelvin-Helmholtz instabilities.

Finally, it was confirmed that the total circulation for a piston–based vortex generator is scaled by the stroke length of the slug-flow out of the exhaust, L_0 and the speed of the flow out of the exhaust, U_0. The circulation of the vortex ring was found to scale with the diameter of the exhaust D_0. For the current set of measurements, the maximum normalised total circulation was found to be $\tilde{\Gamma}_{D_0} \approx 2.5 - 2.7$, whereas the maximum normalised ring circulation was found to be $\tilde{\Gamma}_{D_0} \approx 3.2 - 3.6$.

The authors gratefully acknowledge the Natural Sciences and Engineering Research Council of Canada (NSERC) for funding this work.

REFERENCES

Aydemir, E., Worth, N. A. & Dawson, J. R. 2012 The formation of vortex rings in a strongly forced round jet. *Exp. Fluids* **52** (3), 729–742.

Benjamin, T. B. 1976 Applications of methods of functional analysis to problems in mechanics. *Lecture Notes in Mathematics* **503**, 8–28.

Cater, J. E., Soria, J. & Lim, T. T. 2004 The interaction of the piston vortex with a piston-generated vortex ring. *J. Fluid Mech.* **499**, 327–343.

Didden, N. 1979 On the formation of vortex rings: Rolling-up and production of circulation. *Z. Angew Math. Phys.* **30**, 101–116.

Fernando, J. N. & Rival, D. E. 2016 On vortex evolution in the wake of axisymmetric and non-axisymmetric low-aspect-ratio accelerating plates. *Phys. Fluids* **28**, 017102.

Gan, L. & Nickels, T. B. 2010 An experimental study of turbulent vortex rings during their early development. *J. Fluid Mech.* **649**, 467–496.

Gharib, M., Rambod, E. & Shariff, K. 1998 A universal time scale for vortex ring formation. *J. Fluid Mech.* **360**, 121–140.

Glezer, A. 1988 The formation of vortex rings. *Phys. Fluids* **31**, 3532–3542.

James, S. & Madnia, C. K. 1996 Direct numerical simulation of a laminar vortex ring. *Phys. Fluids* **8**, 2400–2414.

Krieg, M. & Mohseni, K. 2013 Modelling circulation, impulse and kinetic energy of starting jets with non-zero radial velocity. *J. Fluid Mech.* **719**, 488–526.

Krueger, P. S. 2005 An over-pressure correction to the slig model for vortex ring circulation. *J. Fluid Mech.* **545**, 427–443.

Krueger, P. S. 2008 Circulation and trajectories of vortex rings formed from tube and orifice openings. *Physica D* **237**, 2218–2222.

Krueger, P. S. & Gharib, M. 2003 The significance of vortex ring formation to the impulse and thrust of a starting jet. *Phys. Fluids* **15**, 1271–1281.

Lawson, J. M. & Dawson, J. R. 2013 The formation of turbulent vortex rings by synthetic jets. *Phys. Fluids* **25**, 105–113.

Maxworthy, T. 1972 The structure and stability of vortex rings. *J. Fluid Mech.* **51**, 15–32.

Nitsche, M. & Krasny, R. 1994 A numerical study of vortex ring formation at the edge of a circular tube. *J. Fluid Mech.* **276**, 139–161.

Pullin, D. I. 1979 Vortex ring formation at tube and orifice openings. *Phys. Fluids* **22**, 401–403.

Rosenfeld, M., Rambod, E. & Gharib, M. 1998 Circulation and formation number of laminar vortex rings. *J. Fluid Mech.* **376**, 297–318.

Saffman, P. G. 1978 The number of waves on unstable vortex rings. *J. Fluid Mech.* **84**, 625–639.

Shariff, K. & Leonard, A. 1992 Vortex rings. *Annu. Rev. Fluid Mech.* **24**, 235–279.

Zhao, W., Frankel, S. H. & Mongeau, L. G. 2000 Effects of trailing jet instability on vortex ring formation. *Phys. Fluids* **12** (3), 589–596.